RSC Advances

PAPER

View Article Online
View Journal | View Issue

Cite this: *RSC Adv.*, 2017, **7**, 47539

Bifunctional catalyst Pd–Al-MCM-41 for efficient dimerization–hydrogenation of β-pinene in one pot

Song Zhang,†[ab] Chao Xu,†[ab] Guoqing Zhai,[a] Mingliang Zhao,[a] Mo Xian,[a] Yuxiang Jia,[a] Zongjiang Yu,[a] Fusheng Liu,[b] Fangfang Jian*[b] and Weizhi Sun*[a]

Received 3rd August 2017
Accepted 2nd October 2017

DOI: 10.1039/c7ra08569a

rsc.li/rsc-advances

A new type of bimetallic palladium and aluminum incorporated mobile crystalline materials (Pd–Al-MCM-41) as bifunctional catalysts has been hydrothermally synthesized. Characterization shows that these molecular materials exhibit an ordered mesoporous structure, high surface area and a good dispersion of palladium in the frame. The catalytic activity of the Pd–Al-MCM-41 for the dimerization–hydrogenation reaction system of β-pinene in one pot has been systematically studied. $Pd_{0.5}$–Al_{30}-MCM-41 (SiO_2/Al_2O_3 = 30, 0.5 wt% palladium content) was found to be the best catalyst which gave a dimer yield of up to 64.7%. It is worth noting that palladium shows a good synergic catalytic effect with aluminum in the dimerization reaction and enhances the dimerization yield. Furthermore, the bifunctional catalyst displayed a good activity over 4 runs.

1. Introduction

Pinene dimerization reaction has drawn much interest in recent years,[1,2] because the resulting dimers are promising candidates of aviation biofuels.[3,4] According to previous research, the pinene dimers show a high density and net heat combustion comparable to aviation fuel.[3] As a widely distributed natural product, pinene is easily available and has extensive applications in pharmaceutical and cosmetic production.[5] Its intrinsic bicyclic structures possess large ring strain energy which contributes to their high net heat of combustion. The dimerization and hydrogenation give rise to products with higher density and improved combustion properties.[6] All of these make pinene a potential material for the production of aviation biofuels.

Traditional strategies for pinene dimerization usually involve the utilization of Lewis acids or Brφnsted acids as catalysts,[7–9] which results in many problems, such as equipment corrosion, tedious work-up procedures and environmental contamination. Recent research on the applications of heterogeneous catalysts in pinene dimerization facilitated the separation of the products and the recovery of the catalysts. These catalysts include montmorillonite K10, Nafion, phosphotungstic acid, phosphotungstic acid/MCM-41 and Al-MCM-41.[6,9–13] Among all kinds of support materials, silica mesoporous materials draw great interests in recent years due to their ordered structures, high surface area and the flexibility to accommodate various metals and functional groups to achieve different acidities and catalytic properties. Most commonly used silica mesoporous materials are MCM-41,[14–16] SBA-15 (ref. 17) and KIT-6.[18] The former two have ordered hexagonal channels and the latter one is a cubic mesoporous material. MCM-41 has special advantages over the other two materials in dimerization of pinene. Its relatively smaller pore diameter is capable of effectively avoiding the formation of polymers whose molecular size is too large to go through the channel. The pore diameter of MCM-41 is only 2–4 nm, while it is 4–20 nm for SBA-15 and >4 nm for KIT-6. Furthermore, for fuel application, the unsaturated dimers must be hydrogenated to enhance their stability. Hydrogenation of pinene dimerization products is traditionally catalyzed by heterogeneous catalysts, such as supported palladium and nickel.[19,20] To accomplish an efficient synthetic strategy, herein, we have developed a one-pot synthesis strategy: incorporated the bimetallic MCM-41 catalyst as a new type of bifunctional catalyst for the dimerization–hydrogenation reaction system to produce terpane-dimers in one pot, such as Pd–Al-MCM-41, which includes dimerization's active sites and hydrogenation's active sites. The aluminum centers provide Lewis acid sites (and Brönsted acid sites) for the activation of dimerization step while the incorporated palladium promotes the following hydrogenation directly after the dimerization step with the introduction of hydrogen. The mesoporous materials supported bimetallic catalysts have been reported. However, in these researches, the two metal centers usually work synergetically to promote one reaction.[21]

[a]*Key Laboratory of Bio-based Materials, Institute of Biotechnology, Qingdao Institute of Biomass Energy and Bioprocess Technology, Chinese Academy of Sciences, Qingdao 266101, China. E-mail: sunwz@qibebt.ac.cn*

[b]*Qingdao University of Science and Technology, Qingdao 266042, China. E-mail: ffj2013@163.com*

† These authors contributed equally to this work.

Supported catalysts with two active centers to promote independent reactions are rarely reported. In this work, an efficient bifunctional catalyst Pd–Al-MCM-41 has been successfully established for the dimerization–hydrogenation reaction system in one pot.

2. Materials and methods

2.1 Materials and instrumentations

All reagents are AR. Sodium silicate, aluminum sulfate, palladium chloride, palladium acetate and hydrochloric acid were obtained from Sinopharm Chemical Reagent Co. Ltd. 1-Cetyltrimethyl ammonium bromide (CTAB) are obtained from Aladdin Industrial Corporation.

All samples were analyzed by scanning electron microscopy with powder X-ray diffraction (XRD; Bruker D8 Advance), transmission electron microscope (TEM; JEM-2000EX), Fourier transform infrared spectroscopy (FTIR; Thermo Nicolet 8700), pyridine Fourier transform infrared spectroscopy (Py-FTIR; Thermo Nicolet 6700), and Temperature Programmed Desorption (NH_3-TPD, Auto Chem II 2920; CO-TPD, Auto Chem II 2920). The specific surface area and the pore size distribution of all samples were obtained by N_2 adsorption at 77.26 K on a Micrometrics TriStar 3000.[14] XPS analysis was conducted on ThermoScientific K-Alpha X-ray photoelectron spectroscopy.

2.2 Catalyst preparation

Pd–Al-MCM-41 with different SiO_2/Al_2O_3 ratios was synthesized by a hydrothermal method. It was carried out as follows: typically, sodium silicate was added to de-ionized water and stirred until dissolved. The required amount of aluminum sulfate was introduced slowly under stirring and stirring was continued for 1 h after the introduction, followed by the addition of aqueous solution of palladium nitrate. The mixture was stirred for another 1 h. Finally, template solution 1-cetyltrimethyl ammonium bromide (CTAB) was added dropwise to the above mixture with stirring in 5 min. The final molar composition of the gel was $SiO_2 : nAl_2O_3 : 0.5CTAB : 120H_2O$ (n = 0.1, 0.05, 0.033, 0.025, 0.01, 0.005). The palladium loadings were 1 wt% (Pd_1–Al-MCM-41) and 0.5 wt% ($Pd_{0.5}$–Al-MCM-41) of the raw materials. The pH value was adjusted to 11 by dilute sulfuric acid (1 mol L^{-1}). The resulting gel was stirred for another 1 h, sealed in an autoclave and heated at 120 °C for 72 h. After cooled to room temperature, the resulting powders were recovered by filtration, washed with an excess of deionized water, dried at 70 °C overnight and calcined at 550 °C in air for 10 h to remove the template.[1]

Palladium chloride was also used as the palladium source as a comparison with palladium nitrate. When palladium chloride was employed, certain amount of concentrated hydrochloric acid was added to aid the dissolution of the salt in water. Pd–Al-MCM-41 catalysts mentioned below were all synthesized from palladium nitrate except those specified.

2.3 The dimerization–hydrogenation reaction of pinene

The dimerization of pinene (β-pinene) was an intense exothermic reaction. In a typical process, slow addition of pinene to the reaction system was considered as the safest method. The dimerization reaction was carried out with a certain amount of catalyst in different reaction times. After that, hydrogen was introduced with a balloon and the reaction continued for 24 h at 100 °C.

2.4 The reusability of the catalyst

The reusability of the catalysts was studied using $Pd_{0.5}$–Al_{30}-MCM-41 as an example. After the dimerization hydrogenation reaction, the reaction system was separated by filtration, washed with ethanol and dried at 100 °C in the drying oven overnight. Afterwards, catalysts were calcined in the tube furnace for 4 h to remove the coke formed on the acid sites.

3. Results and discussion

3.1 Characterization

Generally, good crystallinity and long-range hexagonal mesostructure were formed for all samples except Pd–Al_{10}-MCM-41, which reflected in the low-angle XRD patterns were three strong diffraction peaks that can be indexed to (100), (110) and (200) (Fig. 1).[22,23] TEM image also showed a highly ordered mesoporous structure with long ordered and regular two-dimensional hexagonal pore structures for these samples (Fig. 2). Their N_2 adsorption–desorption isotherms exhibited hysteresis loop of type IV which was typical for regular mesoporous materials (Fig. 3b–f).[24] N_2-adsorption study also showed that these samples had extremely narrow pore size distribution which indicated uniform pore structures (Fig. 4), and their average pore sizes were 3.70–5.12 nm (Table 1). This ordered pore structure ensured the high dimer selectivity, as the narrow pore of the material could effectively inhibit the occurrence of polymerization. CO-chemisorption showed that palladium had a good dispersion in the frame of the materials (Fig. 6). XPS showed that Lewis acidity of aluminium species increased obviously with the introduction of palladium species, and

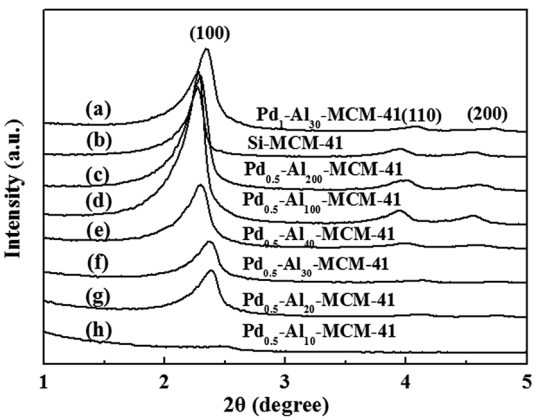

Fig. 1 Low-angle XRD patterns of Pd–Al-MCM-41 catalysts.

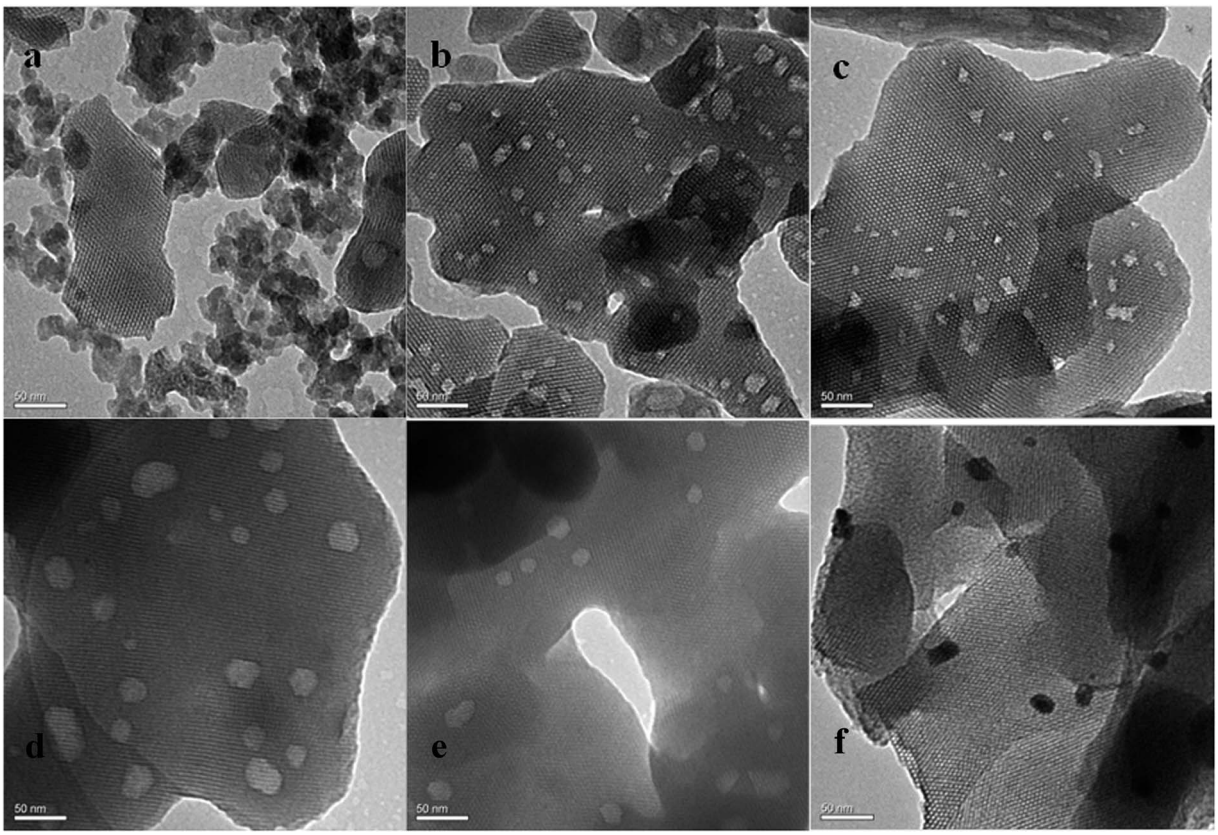

Fig. 2 TEM images: (a–d) are Pd_1–Al-MCM-41 with SiO_2/Al_2O_3 ratios of 10, 20, 100 and 200, respectively; (e) $Pd_{0.5}$–Al_{100}-MCM-41; (f) Pd_1–Al_{100}-MCM-41($PdCl_2$).

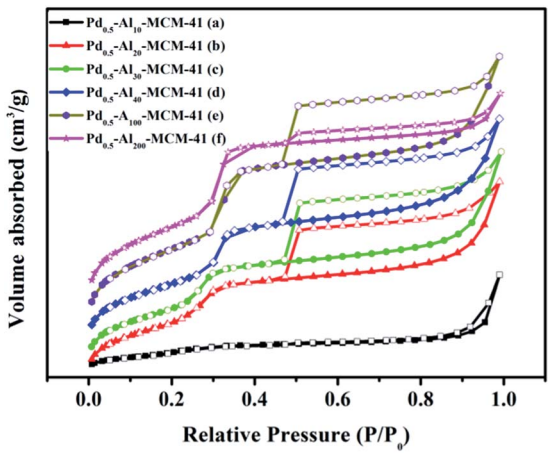

Fig. 3 N_2 adsorption–desorption isotherms.

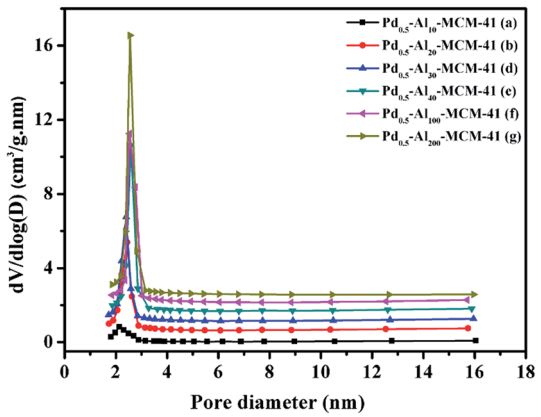

Fig. 4 BJH pore size distribution curve.

palladium mainly existed in frame in form of Pd(II) (Table 3 and Fig. 7). Py-FT-IR showed that the incorporation of a small amount of palladium clearly increased Lewis acid amount of catalyst (Fig. 8).

3.1.1 Influence of aluminum. The influence of aluminum content on the structure properties of these materials was also clearly observed. The intensities of the typical peaks in the low-angle XRD patterns decreased gradually while the ratio of incorporated Al increased. The (100) diffraction peak of became wide and weak with a shift towards higher angles (Fig. 1c–g). The (110) and (200) diffraction peaks disappeared completely when the SiO_2/Al_2O_3 ratio dropped to 10 (Fig. 1h). These indicated that partial destruction to the ordered silica frame occurred when aluminum was introduced into the structure. Large amount of aluminum could even cause frame collapse. This kind of deterioration was also observed from TEM analysis and N_2-adsorption study. In the TEM image, more defects in the

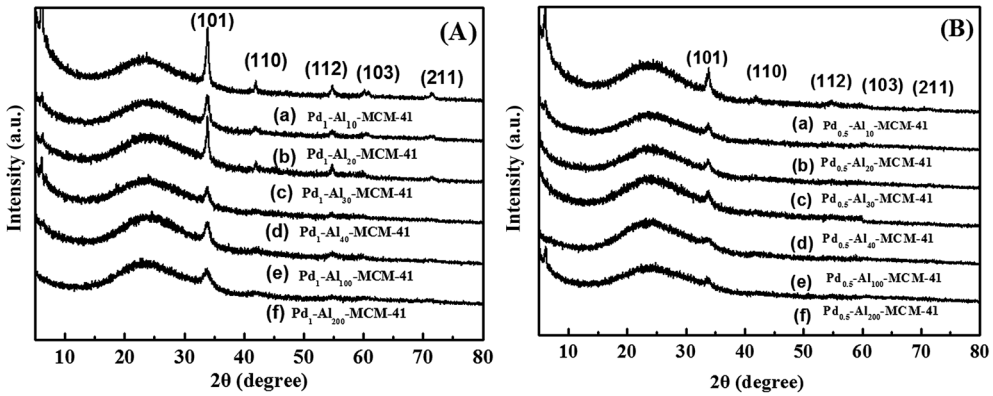

Fig. 5 High-angle XRD patterns of Pd–Al-MCM-41 catalysts.

Table 1 Specific surface area, pore volume and pore size of Pd–Al-MCM-41 catalysts

Entry	SiO_2/Al_2O_3	$Pd(NO_3)_2$ (%)	Surface area ($cm^2\ g^{-1}$)	Pore volume ($cm^3\ g^{-1}$)	Pore size (nm)
1	10	0.5	232.6	0.43	7.39
2	20	0.5	758.4	0.93	4.17
3	30	0.5	785.9	0.99	5.05
4	40	0.5	853.3	1.05	4.94
5	100	0.5	1091.2	1.27	4.65
6	200	0.5	1090.1	1.02	3.75
7	10	1	222.3	0.43	7.77
8	20	1	643.9	0.82	5.12
9	30	1	774.1	0.91	4.68
10	40	1	824.2	1.02	4.94
11	100	1	1055.1	1.15	4.35
12	200	1	961.8	0.89	3.70

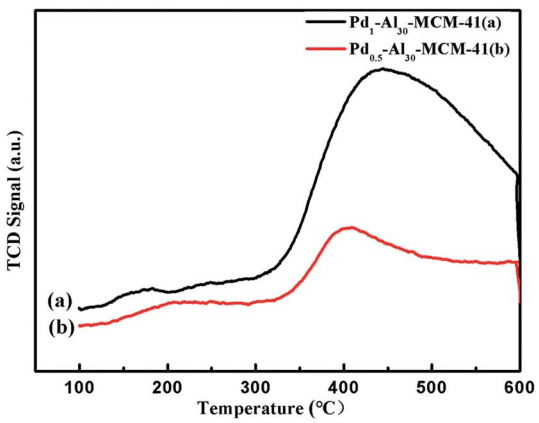

Fig. 6 CO-chemisorption analysis of Pd–Al-MCM-41.

mesostructure were observed as the aluminum content increased (Fig. 2b–d) and severe damage occurred with Pd–Al_{10}-MCM-41 (Fig. 2a). Also, no typical hysteresis loop of type IV was observed in adsorption–desorption isotherm for Pd–Al_{10}-MCM-41 (Fig. 3a) and it showed extremely wild pore size distribution (Fig. 4a) with a low surface area of only about 200 $cm^2\ g^{-1}$ (Table 1, entry 1, 7). All these evidences suggested that the mesostructure was totally destroyed with a low SiO_2/Al_2O_3 ratio of 10. This was probably caused by the difference in Si–O and Al–O bond lengths.[25] When the large amount of aluminum was introduced, severe structural distortion occurred. These structure changes caused by the incorporation of aluminum had great influence on the catalytic property of the catalysts. Pd–Al_{10}-MCM-41 showed low catalytic activity than other catalysts with good mesostructure.

Besides the structural changes, the incorporation of Al also introduced strong acidic sites into the frame according to the NH_3-TPD experiments. The amount of strong acidic sites increased as the Al content increases (Table 2). The enhancement in acidic sites generated higher catalytic activity towards dimerization of pinene and an obvious increase tendency was observed in the yield of dimer with increasing acidic sites.

3.1.2 Influence of palladium. Palladium also displayed significant influences on the structural properties of the materials. Differences in peak intensity were observed with the variation of Pd loadings and sources in high-angle XRD. Pd_1–Al-MCM-41 series (Fig. 5A) exhibited stronger peaks in comparison with $Pd_{0.5}$–Al-MCM-41 series (Fig. 5B). This was probably because higher Pd loading increased the Pd–O particles outside the mesoporous frame. Compared to palladium nitrate, palladium chloride gave stronger Pd–O diffraction peaks, suggesting a poor dispersion of the palladium particles due to the poor solubility of the salt in water. Furthermore, obvious aggregation was observed as black particles on the TEM image for Pd_1–Al_{100}-MCM-41 ($PdCl_2$) (Fig. 2f) while a better dispersion was achieved when palladium nitrate was employed (Fig. 2c). High palladium content seemed also to block the channels of the materials because smaller surface areas were detected for Pd_1–Al-MCM-41 series (Table 1, entry 7–12).

CO-chemisorption analysis of $Pd_{0.5}$–Al_{30}-MCM-41 was showed in Fig. 6, from the room temperature to 450 °C, CO absorbed in the surface of the catalyst showed transition peaks at 200 °C and gradual desorption peaks at 400 °C, it indicated that palladium had a good dispersion in the frame of the materials, which ensured the high catalytic activity in hydrogenation.

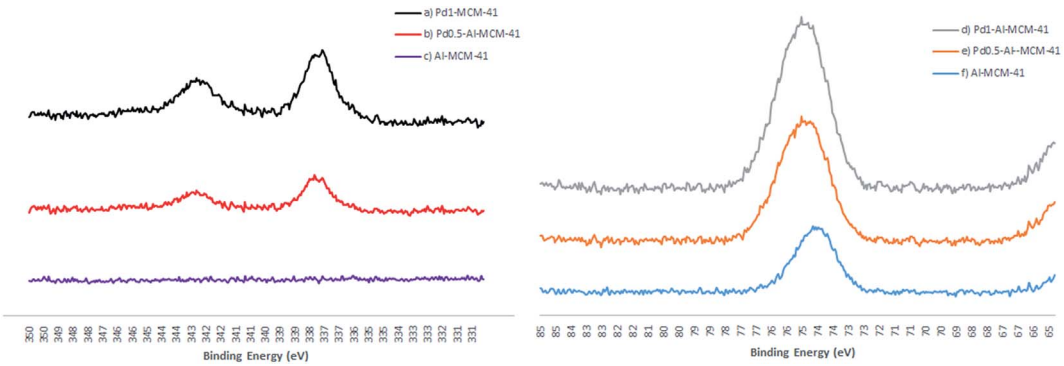

Fig. 7 XPS experiments: (a) the electron binding energy of Pd 3d of Pd_1–Al_{30}-MCM-41; (b) the electron binding energy of Pd 3d of $Pd_{0.5}$–Al_{30}-MCM-41; (c) the electron binding energy of Pd 3d of Al_{30}-MCM-41; (d) the electron binding energy of Al 2p of Pd_1–Al_{30}-MCM-41; (e) the electron binding energy of Al 2p of $Pd_{0.5}$–Al_{30}-MCM-41; (f) the electron binding energy of Al 2p of Al_{30}-MCM-41.

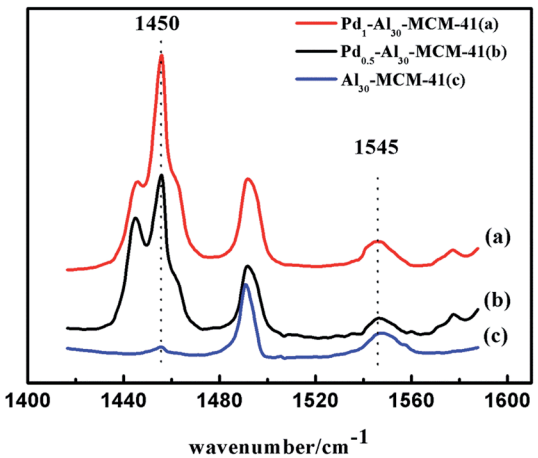

Fig. 8 IR spectra of pyridine adsorbed on samples.

Table 2 TPD of NH_3 result of the Pd–Al-MCM-41

SiO_2/Al_2O_3	$Pd(NO_3)_2$ (%)	Surface acid sites (mmol g^{-1}) 180–200 °C	600–700 °C	Total surface acid sites (mmol g^{-1})
—	—	—	—	0.169
10	0.5	0.475	0.169	0.616
20	0.5	0.489	0.141	0.613
30	0.5	0.486	0.124	0.625
40	0.5	0.456	0.139	0.623
100	0.5	0.421	0.167	0.638
200	0.5	0.403	0.217	0.621
10	1	0.391	0.218	0.516
20	1	0.469	0.125	0.581
30	1	0.457	0.112	0.579
40	1	0.450	0.122	0.577
100	1	0.413	0.127	0.579
200	1	0.391	0.166	0.562

As shown in Table 3 and Fig. 7, XPS experiments showed that the electron binding energy of Al 2p increased from 74.56 eV to 74.74 eV with the incorporation of 0.5% palladium content,

Table 3 The electron binding energy of samples[a]

Samples	Calcination temperature (°C)	BE Pd 3d (eV)	BE Al 2p (eV)
Al-MCM-41	550	—	74.56
$Pd_{0.5}$–Al-MCM-41	550	336.9	74.74
Pd_1–Al-MCM-41	550	336.9	74.68

[a] The binding energy can be set at C 1s = 284.8 eV.

which indicated that the electron cloud density of aluminium species decreased and Lewis acidity was strengthened, it is easier to promote ethylenic-bond polarization and catalytic electrophilic addition. Therefore, the introduction of palladium generates a synergistic catalysis effect. However, when the palladium content was increased to 1%, the electron binding energy of Al 2p only increased from 74.56 eV to 74.68 eV. This explained that a large amount of palladium may destroy the mesoporous structure but had a negative effect on the increase of Lewis acidity. The binding energy of Pd 3d was 336.9 eV after calcination at 550 °C, corresponding standard value ((BE) PdO = 337.0 eV), which suggested that palladium species existed mainly in the form of highly dispersed PdO particles in the mesoporous frame. In addition, Pd(II) also showed a good catalytic activity for the hydrogenation reaction.

Besides the structural influence, palladium content also affected the total acidity of the materials. According to the NH_3-TPD experiments, the high palladium content of 1% caused an average decline of 9% in the total acidic sites compared with 0.5% palladium content (Table 2). This was probably associated with the increased Pd–O particles outside the mesoporous frame with the Pd_1–Al-MCM-41 series and channel block caused by these particles may hinder the absorption of NH_3.

As shown in Fig. 8, Py-FT-IR experiments showed that obvious enhancement was observed for both acid sites, especially Lewis acid sites, after the introduction of palladium. This result was consistent with the XPS analysis. It was believed that the incorporation of palladium would alter the electronic density of aluminum thus enhancing its Lewis acidity. This

enhancement was reflected in a yield increase of the dimerization reaction.

3.2 Catalytic activity of Pd–Al-MCM-41

3.2.1 Catalyst screening. Reactions were carried out with three series of catalysts, Pd_1–Al-MCM-41, $Pd_{0.5}$–Al-MCM-41 and Al-MCM-41, at 100 °C with a catalyst loading of 2 wt% for 2 h.

As shown in Fig. 9, the dimer yields of $Pd_{0.5}$–Al-MCM-41 and Al-MCM-41 series displayed similar variation tendency as the SiO_2/Al_2O_3 ratio changed. Both of the catalysts with a low SiO_2/Al_2O_3 ratio of 10 exhibited very poor dimerization activity. According to the characterization above, these two samples had severe structural damages and their surface areas and pore volumes were dramatically reduced due to the structure collapse. This indicated that the catalytic activity was closely related to the mesostructure of the material. For other samples, the yields of dimers generally declined as the SiO_2/Al_2O_3 ratio increased from 20 to 200. According to the NH_3-TPD experiments, the amount of strong acidic sites decreased as Al content was reduced. It was clear that strong acidic sites played a key role in the catalytic activity of mesoporous materials for dimerization of pinene (Fig. 10).

Interestingly, the introduction of 0.5% of Pd into the frame increased the dimer yields rather than caused a decline as expected. This showed sign of possible synergetic effect between Pd and Al on dimerization activity, which Lewis acidity of Al increased obviously due to electronic effect of Pd. However, higher Pd content of 1% caused severe yield decline (Fig. 9). Higher Pd loading increased the Pd–O particles outside the mesoporous frame and these particles may block the channel of the mesomaterials causing smaller surface areas, thus lowered the yields.

3.2.2 Condition screening. A series of experiments were carried out with different catalyst dosages, reaction temperatures and time using $Pd_{0.5}$–Al_{30}-MCM-41 as catalyst. The yield of dimers quickly increased from 0.55% to 64.7% as the mass ratio of catalyst/pinene ranged from 0 to 0.020 at 140 °C in a reaction time of 2 h. And the increase slowed down when the catalyst dosages above 2% (Table 4, entry 1–6). Temperature also had influence on the generation of dimers. The yield of dimers increased as the reaction temperature rose from 100 to 160 °C and then slightly declined at 180 °C with a catalyst dosage of 2% in 4 h (Table 4, entry 7–10).

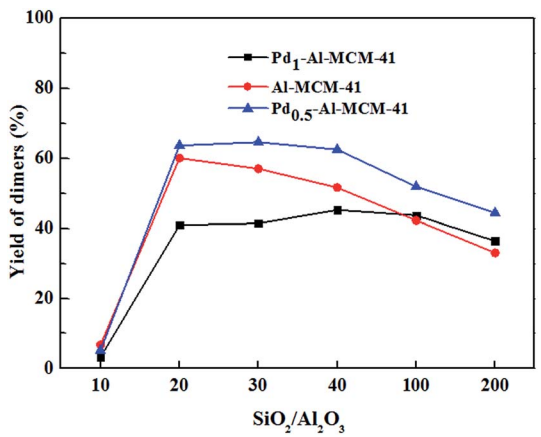

Fig. 9 Catalysts with different SiO_2/Al_2O_3 ratios for dimerization of β-pinene. Reaction conditions: β-pinene 10 g, catalyst 0.2 g, 2 h, 140 °C.

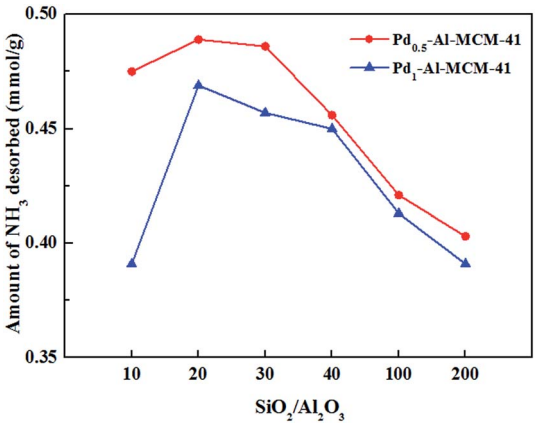

Fig. 10 Acid amount of catalysts with different SiO_2/Al_2O_3 ratios.

Table 4 Condition screening of dimerization of β-pinene

Entry	Catalyst dosage (%)	Temperature (°C)	Time (h)	Dimers (%)	Isomers (%)	Conversion (%)
1	0	140	4	0.6	14.9	15.5
2	0.5	140	4	44.7	42.5	89.6
3	1	140	4	53.8	33.2	91.6
4	2	140	4	64.7	21.8	91.8
5	3	140	4	64.7	20.6	90.0
6	4	140	4	65.6	19.9	90.0
7	2	100	4	38.0	43.3	82.4
8	2	120	4	46.6	39.7	87.7
9	2	160	4	56.7	25.6	88.7
10	2	180	4	54.2	26.6	88.6
11	2	140	0.17	19.3	53.6	73.3
12	2	140	0.5	32.2	44.9	78.0
13	2	140	1	38.3	40.8	80.5
14	2	140	2	58.6	25.6	87.2
15	2	140	8	68.1	18.6	92.3
16	2	140	16	67.5	15.3	94.2

Reaction monitoring found that isomerization occurred much faster than dimerization. Isomers were detected within 10 min and they took up 53.6% in the products with a dimer yield of only 19.3% (Table 4, entry 11). Most of the isomers were gradually converted into dimers with time and the yield of dimers reached 68.1% in a reaction time of 8 h (Table 4, entry 11–15). When the reaction time was prolonged to 16 h, a slight drop in the dimer yield was observed due to the generation of oligomers (Table 4, entry 16).

3.2.3 One pot dimerization–hydrogenation of pinene. One-pot dimerization–hydrogenation of pinene was carried out using $Pd_{0.5}$–Al_{30}-MCM-41 as catalyst with a dosage of 2%. The dimerization process was carried out at 140 °C for 4 h which was considered to be the most efficient condition and after the dimerization, hydrogen was introduced and the reaction maintained at 60 °C for 24 h. The mass spectrometry showed

that dimerization–hydrogenation products of pinene were mainly composed of compounds with molecular weight of 272, and a few compounds are of molecular weights of 274 and 276. This hydrogenation result was consistent with that reported in the literature.[3] FI-IR analysis result showed that the bands between 1600 and 1700 cm^{-1} appear absorption peaks (Fig. 11) and ^{1}H-NMR result revealed that there were a few vibration peaks with a chemical shift of 4–6 ppm (Fig. 12). These results indicated that hydrogenation reaction of dimer almost completed with a few unsaturated bonds left.[26] The catalyst displayed good activity for one-pot dimerization–hydrogenation of pinene and gave a total yield of 63.9% (Table 5, entry 1). After the reaction, the catalyst was separated from the reaction system by filtration, washed with ethanol, dried overnight in the drying oven at 100 °C, calcined in the tube furnace at 500 °C for 4 h and reused for the reaction. The catalyst maintained its catalytic activity during recycling and no remarkable yield decline was observed after the catalyst was reused for four times (Table 5, entry 2–5), which showed that Pd–Al-MCM-41 had a very good reusability.

3.2.4 Mechanism. As mentioned above, the catalytic activity is closely related to the quantity of acidic sites in the materials. Both the Lewis acid sites and Brönsted acid sites can promote the dimerization reaction. Isomerization occurred through protonation of β-pinene before the dimerization reaction. Possible isomers include α-pinene, limonene and camphene as well as some aromatic compounds such as cymene (Scheme 1).

The mixture of the isomers further went through the dimerization reaction to form a mixture containing different combinations of isomers. Possible catalytic pathways catalyzed by the Brönsted acid sites and the Lewis acid sites are shown in Scheme 2 and 3 using β-pinene as the substrate. In the catalytic pathway by Brönsted acid, the pinene was promoted by a proton originated from the bridge hydroxyl of the [≡Si···(OH)···Al≡] unit. The active Lewis acidic species were not clear update and it was rational that the empty orbital in the active Lewis acid sites would induce the formation of carbonium ion and boost the

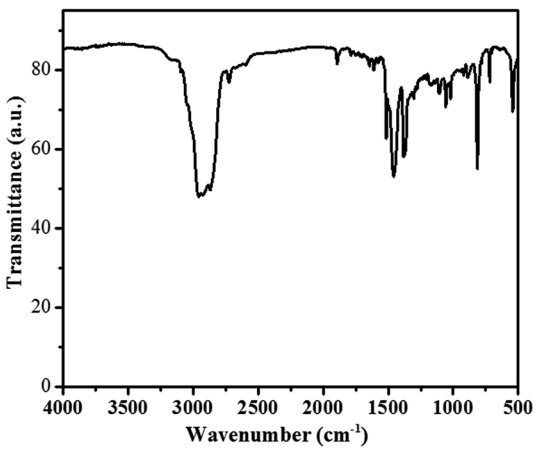

Fig. 11 FT-IR of products catalyzed by $Pd_{0.5}$–Al_{30}-MCM-41.

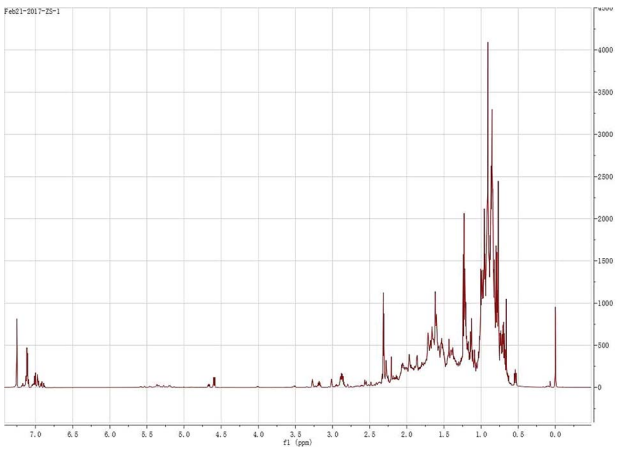

Fig. 12 ^{1}H-NMR of products catalyzed by $Pd_{0.5}$–Al_{30}-MCM-41.

Table 5 One-pot dimerization–hydrogenation of pinene and catalyst reusability

Times	Yield of dimer (%)	Conversion (%)
1	63.9	90.2
2	62.5	88.5
3	61.6	87.8
4	60.7	85.3
5	57.5	82.2

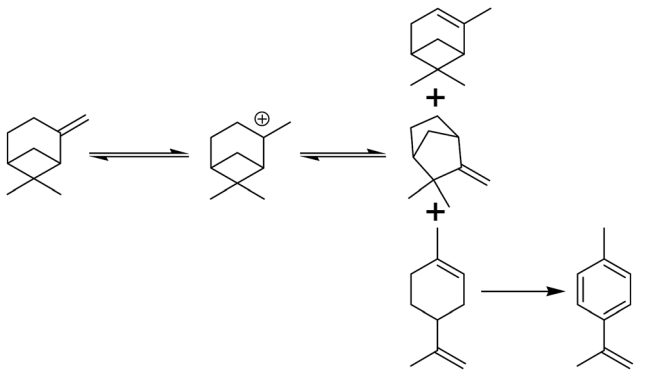

Scheme 1 Isomerization of β-pinene.

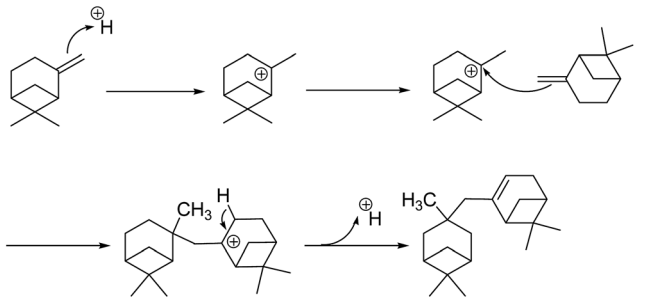

Scheme 2 Possible catalytic pathway by Brönsted acid sites of Pd–Al-MCM-41.

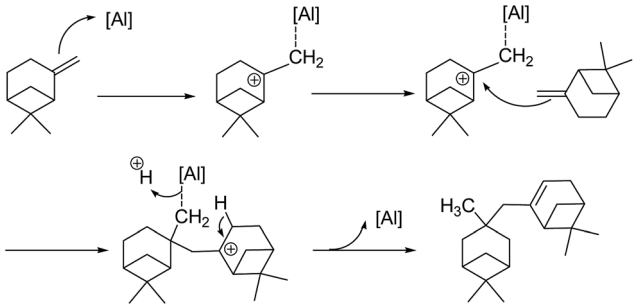

Scheme 3 Possible catalytic pathways by Lewis acid sites of Pd–Al-MCM-41.

dimerization process.[27] The existence of palladium played a synergetic effect by increasing the Lewis acidity of aluminium species.

4. Conclusions

In this study, bifunctional catalysts Pd–Al-MCM-41 have been successfully synthesized by a hydrothermal method. The catalysts have been characterized by N_2-adsorption, XRD, XPS, FTIR and TEM analyses. The results showed that these catalysts have ordered mesoporous structure and high surface area and a good dispersion of palladium in the frame. These catalysts successfully promoted dimerization of β-pinene and the following hydrogenation step in one pot in mild condition. The influence of palladium and aluminum loadings has been well studied and $Pd_{0.5}$–Al_{30}-MCM-41 with palladium nitrate as palladium source is found to be the best catalyst. These catalysts display good activity over 4 runs. In summary, the new types of bifunctional catalysts (Pd–Al-MCM-41) have a good application prospect in a dimerization–hydrogenation one-pot reaction system to produce aviation biofuels.

Conflicts of interest

The authors declare no competing financial interest.

Acknowledgements

This study is supported by the Natural Science Foundation of Shandong Province. Grant Number: ZR2016BQ39.

References

1 J. J. Zou, N. Chang, X. Zhang and L. Wang, *ChemCatChem*, 2012, **4**, 1289–1297.
2 K. Kristensen, T. Cui, H. Zhang, A. Gold, M. Glasius and J. D. Surratt, *Atmos. Chem. Phys.*, 2014, **14**, 4201–4218.
3 B. G. Harvey, M. E. Wright and R. L. Quintana, *Energy Fuels*, 2010, **24**, 267–273.
4 T. K. Hari, Z. Yaakob and N. N. Binitha, *Renewable Sustainable Energy Rev.*, 2015, **42**, 1234–1244.
5 A. A. Tzialla, I. V. Pavlidis, M. P. Felicissimo, P. Rudolf, D. Gournis and H. Stamatis, *Bioresour. Technol.*, 2010, **101**, 1587–1594.
6 M. N. Andrea, A. M. Cecilia, C. N. Alejandra, P. E. Natalia and P. M. Isabel, *Curr. Catal.*, 2014, **3**, 240–243.
7 R. Dimitrova, G. Gündüz and M. A. Spassova, *J. Mol. Catal. A: Chem.*, 2006, **243**, 17–23.
8 C. M. López, F. J. Machado, K. Rodríguez, D. Arias, B. Méndez and M. Hasegawa, *Catal. Lett.*, 1999, **62**, 221–226.
9 I. L. Simakova, Y. S. Solkina, B. L. Moroz, O. A. Simakova, S. I. Reshetnikov, I. P. Prosvirin, V. I. Bukhtiyarov, V. N. Parmon and D. Y. Murzin, *Appl. Catal., A*, 2010, **385**, 136–143.
10 G. Nie, J. J. Zou, F. Ren, X. Zhang and W. Li, *Catal. Today*, 2014, **234**, 271–277.
11 B. G. Harvey, M. E. Wright and R. L. Quintana, USA 8227651, 2010.
12 L. Brožová, J. Žitka, P. Sysel, Š. Hovorka, A. Randová, J. Storch, M. Kačírková and P. Izák, *Desalin. Water Treat.*, 2015, **55**, 2967–2972.
13 Z. Liu, S. Cao, S. Wang, W. Zeng and T. Zhang, *React. Kinet., Mech. Catal.*, 2014, **111**, 577–590.
14 X. Xu, C. Song, J. M. Andresen, B. G. Miller and A. W. Scaroni, *Energy Fuels*, 2017, **16**, 1463–1469.
15 Y. Guo, D. Liu, Y. Zhao, B. Gong, Y. Guo and W. Huang, *J. Taiwan Inst. Chem. Eng.*, 2017, **71**, 537–545.
16 A. Corma, V. Fornes, M. T. Navarro and J. J. Perezpariente, *Catalysis*, 1994, **148**, 569–574.
17 S. Wei, H. He, Y. Cheng, C. Yang, G. Zeng and Q. Lu, *RSC Adv.*, 2016, **6**, 103253–103269.
18 S. Wei, H. He, Y. Cheng, C. Yang, G. Zeng, L. Kang, H. Qian and C. Zhu, *Fuel*, 2017, **200**, 11–21.
19 Á. Mastalir, B. Rác, Z. Király and Á. Molnár, *J. Mol. Catal. A: Chem.*, 2007, **264**, 170–178.
20 M. M. L. R. Carrott, F. L. Conceição, J. M. Lopes, P. J. M. Carrott, C. Bernardes, J. Rocha and F. R. Ribeiro, *Microporous Mesoporous Mater.*, 2006, **92**, 270–285.
21 L. Fu, C. Huo, X. He and H. Yang, *RSC Adv.*, 2015, **5**, 20414–20423.
22 Y. Wan, J. Ma, Z. Wang and W. Zhou, *Microporous Mesoporous Mater.*, 2004, **76**, 35–40.
23 Y. Cesteros and G. L. Haller, *Microporous Mesoporous Mater.*, 2001, **43**, 171–179.
24 C. Sangwichien, G. L. Aranovich and M. D. Donohue, *Colloids Surf., A*, 2002, **206**, 313–320.
25 J. B. Jones, *Acta Crystallogr., Sect. A: Cryst. Phys., Diffr., Theor. Gen. Crystallogr.*, 1968, **24**, 355–358.
26 S. K. Lee, H. Chou, T. S. Ham, T. S. Lee and J. D. Keasling, *Curr. Opin. Biotechnol.*, 2008, **19**, 556–563.
27 J. Lu, M. Kamicaito, M. Sawamoto, T. Hicashimura and Y.-X. Deng, *J. Appl. Polym. Sci.*, 1996, **61**, 1011–1016.

